RSC Advances

PAPER

View Article Online
View Journal | View Issue

Cite this: *RSC Adv.*, 2022, **12**, 21255

Study on the effect of solvent on cocrystallization of CL-20 and HMX through theoretical calculations and experiments

Xitong Zhao,[a] Jizhen Li,[a] Shuxin Quan,[b] Xiaolong Fu,*[a] Saiqin Meng,[a] Liping Jiang[a] and Xuezhong Fan*[a]

Cocrystallization is a helpful method for explosives design. However, lack of understanding of the cocrystallization mechanism leads to inefficiency in cocrystal preparation. Therefore, studying the effects of solvent on cocrystal is of great importance for the efficient application of 2,4,6,8,10,12-hexanitrohexaazaisowurtzitane (CL-20). In this paper, the effect of solvent on cocrystallization is investigated by the CL-20/HMX cocrystal/solvent cluster model, the CL-20/HMX/solvent mixture model, the CL-20/HMX cocrystal/solvent interface model combined with quantum chemistry and molecular dynamic methods. The authors find that the hydrogen bond between CL-20 and 1,3,5,7-tetranitro-1,3,5,7-tetrazocane (HMX) is the strongest and the binding energy of cocrystal and solvent molecules is the weakest in ethyl acetate (EA) solvent, indicating that CL-20 and HMX tend to be combined together and there is less hindrance by solvent molecules. Analysis of the CL-20/HMX/solvent mixture and mass density distribution studies show that the solvent effect has a great influence on the crystal faces and the cocrystallization rate of CL-20 and HMX is the highest in EA solvent. The XRD and SEM characterization results are consistent with the theoretical calculations. The present work on the effects of solvent on CL-20/HMX cocrystals is beneficial for understanding the mechanism of the growth of energetic cocrystal materials. It is helpful in selecting more suitable theoretical and experimental conditions and makes access to excellent cocrystals more efficient.

Received 17th June 2022
Accepted 19th July 2022

DOI: 10.1039/d2ra03730k

rsc.li/rsc-advances

1 Introduction

Energetic materials have been widely used in the military and civilian fields. 2,4,6,8,10,12-Hexanitrohexaazaisowurtzitane (CL-20), as one of the most powerful explosives available for practical application at present, exhibits a better oxygen balance, detonation velocity and detonation pressure than most of the widely used explosives.[1] However, the high sensitivity of CL-20 has distinctly limited its application prospects.[2] Therefore, researchers are committed to seeking novel materials with high energy and low sensitivity. Cocrystallization as an attractive crystal engineering strategy can effectively reduce the sensitivity and has been successfully applied in various fields.[3] A cocrystal is normally stabilized by noncovalent interactions, such as hydrogen bonds, π–π stacking and van der Waals interactions.[4,5] In cocrystals, the degree of hydrogen bonding is increased and the CH···O contact distances in them are short among hydrogen bonds, and are similar to those of the insensitive energetic materials 1,1-dinitro-2,2-diaminoethylene (FOX-7) and 2,4,6-triamino-1,3,5-trinitrobenzene (TATB), while the detonation properties can maintain a high level.[6] The balance of energy density and sensitivity is achieved. Since the first synthesis of cocrystals of 2,4,6-trinitrotoluene (TNT) with aromatic nonenergetic materials by Matzger in 2010,[7] cocrystallization of energetic materials has proved a new option for the design and preparation of explosives with both high energy and low sensitivity.

It is advisable to introduce cocrystallization techniques to reduce the sensitivity of CL-20 without decreasing energy. In 2011, Bolton *et al.*[8] prepared CL-20/TNT cocrystal by growth from ethanol solutions, appearing as thick colorless prisms. Gao and coworkers[9] successfully prepared a rod-like CL-20/1,3,5-trinitro-1,3,5-triazacyclo-hexane (RDX) cocrystal with a molar ratio of 1 : 1 by solvent evaporation method. Xu *et al.*[10] prepared a CL-20/1,3,5-triamino-2,4,6-trinitrobenzene (TATB) cocrystal with an average particle size of about 3–5 μm through a rapid nucleation solvent/non-solvent process. By now, CL-20 has been found to form cocrystals with a number of other explosives.[11–17] Although those excellent cocrystals were obtained, the existing preparation methods were still based on a trial-and-error method and cannot realize design or directional preparation of cocrystals completely. It is necessary to understand the competitive relationship between cocrystal and the separate crystals and the formation mechanism of the cocrystal. In recent years, computational method has been proved as a reliable way in materials science research, especially in studying the mechanism of cocrystal.[18–28] Li and coworkers[22] revealed the existent of hydrogen bonds and

[a]Xi'an Modern Chemistry Research Institute, Xi'an 710065, Shaanxi, China. E-mail: fuxiaolong204@163.com

[b]Qingyang Chemical Industry Corporation, Liaoyang 111001, Liaoning, China

van der Waals interactions between CL-20 and TNT molecules in cocrystal based on the density functional theory. Feng *et al.*[23] successfully predicted the most stable molar ratio of CL-20/FOX-7 cocrystal by molecular dynamics (MD) methods.

Due to the excellent properties of 1,3,5,7-tetranitro-1,3,5,7-tetrazocane (HMX) and its wide application in propellant,[29,30] CL-20/HMX cocrystal has attracted a lot of attention of investigators. Bolton *et al.* reported the cocrystal of CL-20 and HMX, exhibiting a plate habit, and noted that there are CH···O type of hydrogen bonds between CL-20 and HMX molecules.[6] The theoretical detonation velocity of CL-20/HMX cocrystal (9484 m s^{-1}) is much higher than HMX, the shock sensitivity reduced to similar with HMX as well. Sun *et al.*[19] simulated the structure of CL-20, HMX, CL-20/HMX cocrystal and its composite by molecular dynamics way and proved that cocrystal of CL-20 and HMX is more stable compared with the composite because of the stronger hydrogen bonds. This laid the foundation for the further study of CL-20/HMX cocrystal energetic materials. During the growth process of CL-20/HMX cocrystal, the solvent selection has a great influence on the cocrystal. Sun *et al.*[31] studied the transitions from CL-20 and HMX to cocrystal in solvent. It is found that the formation of CL-20/HMX cocrystal experiences a significant coformers converting process from separated precipitation to cocrystal in acetone solvent. The effects of solvent on energetic crystals have been preliminary explored both in theoretical and experimental ways. However, the previous works are not deep and comprehensive, and there is little research on the mechanism of cocrystallization.

In our previous study,[32] the inducing effect of nitrate easter on CL-20/HMX cocrystal in solid propellant was investigated through molecular dynamic method combined with a CL-20/HMX/solvent mixture model. However, the simulation method is monotonous and only focus on nitrate ester solvent, the range of simulation and diversity of solvent can be further expanded. To further study the effects and to reveal the mechanism of solvent on CL-20/HMX cocrystal, three common solvents ethyl acetate (EA), acetone (AC) and ethanol (EtOH) were selected in calculation and experiment. We introduced CL-20/HMX cocrystal/solvent cluster model, CL-20/HMX/solvent mixture model, CL-20/HMX cocrystal/solvent interface model combined with quantum chemistry and molecular dynamics way to calculate the properties. The interaction between CL-20 and HMX as well as the binding energy between cocrystal and solvent were investigated. The analysis on CL-20/HMX/solvent mixture showed the cocrystallization rate in different solvents. Moreover, the attachment energy and solvent distribution further explained the effects of solvent on cocrystal. What's more, the theoretical results were well confirmed by experiments. We have a deeper understanding of the effects and mechanism of solvents on CL-20/HMX cocrystal.

2 Methods

2.1 Computation details

2.1.1 Quantum chemistry. In this paper, the molecular structures used in quantum chemistry calculation were constructed with the Genmer component in Molclus program.[33] A CL-20/HMX cocrystal/solvent cluster model with core–shell structure contains a pair of CL-20/HMX cocrystal molecules and 40 solvent molecules was obtained. Then, Molclus together with GFN-xTB[34,35] was employed to search the configuration which with the lowest energy among the 20 cluster structures, that is, the molecular model required for later calculation.

All quantum chemistry calculations are run by ORCA 5.0 program.[36,37] The density functional theory (DFT) method B3LYP[38] with the def2-SV(P) basis[39,40] set was employed to perform the geometry optimization and energy analysis. The binding energy considering counterpoise correction between cocrystal molecules and three different solvents can be obtained in this way. Based on the calculation results, the Multiwfn 3.8 program was used to analysis the wavefunction, it is an extremely powerful wavefunction analysis code, and to do energy decomposition analysis based on molecular force field (EDA-FF).[41] All pictures about molecular structure were created in VMD 1.9.3 program[42] based on Multiwfn output files, as shown in Fig. 1(a)–(c).

2.1.2 Molecular dynamics. The CL-20/HMX cocrystal structure is constructed according to cell parameters obtained from CCDC database. The mass fractions of ε-CL-20, β-HMX and solvent molecules was obtained from experimental data. All calculation and simulation are conducted through applying Materials Studio (MS) 8.0 software. The CL-20/HMX/solvent mixture model contains CL-20, HMX and solvent molecules with a mass ratio of 20 : 20 : 10 matched with the experiment, as shown in Fig. 1(d)–(f).

The CL-20/HMX cocrystal/solvent interface model consisted of a growth surface structure cleaved from 3 × 3 × 3 cocrystal supercell and a solvent layer, which contains 300 EA molecules, 500 AC molecules and 500 EtOH molecules respectively. The solvent layer was placed above the cocrystal layer along the *Z* direction which was set a 3 Å vacuum layer between them, and the vacuum thickness above the solvent layer was set to 50 Å to eliminate possible boundary effects.[43]

Firstly, the structure of the model was optimized, molecular dynamics simulation was carried out according to the optimized stable configuration, NVT ensemble was selected under the COMPASS force field,[44–46] the temperature was set to 298 K, and Anderson was selected as the temperature control method.[47] Considering the accuracy of the calculation results and configuration, the total simulation time of the calculation was set to 1000 ps, the time step is 1.0 fs. The first 200 ps trajectory was employed for the structural relaxation and the other part of trajectory was analyzed. Electrostatic and van der Waals interactions were calculated by Ewald and atom-based methods respectively, with a cutoff radius of 12.5 Å.

2.2 Chemicals and reagents

HMX material was provided by Gansu Yinguang Chemical Industry Co. Ltd. of China. CL-20 material was provided from Qingyang Chemical Industry corporation. Ethyl acetate was purchased from Chengdu Kelong Chemical Reagent Factory. Acetone was provided by Sichuan Xilong Scientific Co., Ltd. of China. Ethanol was purchased from Sinopharm Chemical Reagent Factory.

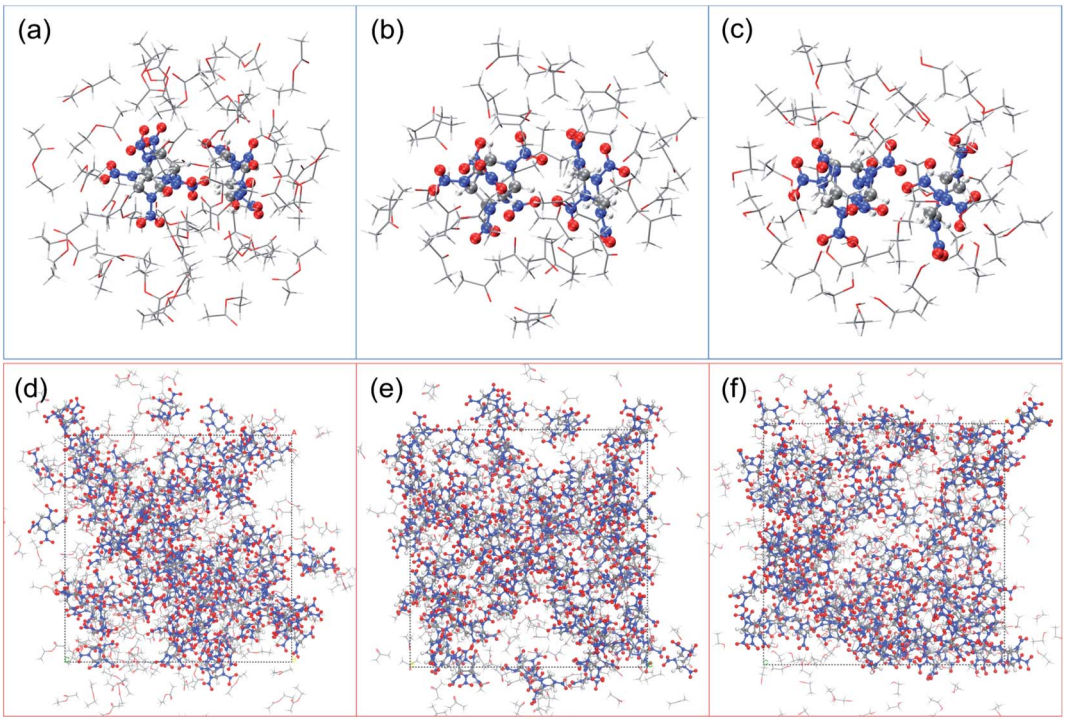

Fig. 1 Cluster structures used in quantum chemistry calculation: (a) EA, (b) AC, (c) EtOH; mixed molecular structure used in molecular dynamics calculation: (d) EA, (e) AC, (f) EtOH. C, H, O, and N atoms are labeled as gray, white, red, and blue, respectively.

2.3 Sample preparation

The preparation of CL-20/HMX cocrystal was carried out at room temperature. First of all, 12 mL solvent was added into 1.1 g ε-CL-20 and 0.37 g β-HMX with a molar ratio of 2 : 1 in glass vails. Then, cocrystals were prepared by evaporation of solvents at natural rate. Finally, a random sample was taken to investigate the composition and content of CL-20, HMX and cocrystal obtained in different solvents.

2.4 Characterization methods

The crystal structure was analyzed using X-ray diffraction (XRD, PANalytical Empyrean) with Cu K_α radiation ($\lambda = 1.54059$ Å). XRD quantitative analysis method is also applied in this paper. The Internal Standard Method (ISM)[48,49] is employed to obtain the content of each phase in the cocrystal formation process. In this experiment, α-Al_2O_3 was added to each sample as a known weight fraction of internal standard substance.

Morphological studies were performed with scanning electron microscopy (SEM, Quanta 600F, 20 kV). Crystal morphologies in this paper were studied by SEM method to tell the difference between cocrystal samples obtained in different solvents.

3 Results and discussion

3.1 Theoretical calculation

3.1.1 Interaction analysis. As mentioned above, in cocrystal, the interactions between CL-20 and HMX are mostly weak interactions. By investigating the type and strength of the weak interaction between cocrystal molecules, the binding trend of cocrystal molecules in solvents can be judged.

In Fig. 2(a), we plotted the interaction region indicator (IRI) maps[50] for CL-20/HMX cocrystal molecules. The isosurface reveal that there are van der Waals interaction and hydrogen bond between CL-20 and HMX molecules. In order to deeply study the change of the interaction of cocrystal molecules in different solvents, the core-valence bifurcation (CVB) index was introduced to investigate the strength of hydrogen bonds.[51–53] The more negative the CVB index, the stronger the hydrogen bond. The CVB index of strong hydrogen bonds is generally negative. The CVB index of medium-strength hydrogen bond is generally around 0 and the CVB index of weak hydrogen bonds is generally positive. The hydrogen bonds between CL-20 and HMX are marked in Fig. 2(b)–(e). The bond length of them is marked in blue and the CVB index of the strongest one is marked in red. Compared with the initial cocrystal, the distance between CL-20 and HMX molecules in the solvent becomes shorter. It is worth noting that the bond strengths of the strongest hydrogen bonds of cocrystal molecules in the EA, AC and EtOH solvents are 0.0409, 0.0414 and 0.0516 in CVB index respectively, which are lower than 0.0624 in the initial cocrystal, that is, the hydrogen bond is stronger. Such result indicates that CL-20 and HMX molecules are more likely to form cocrystal in solvent than in vacuum, especially in EA and AC solvent.

3.1.2 Binding energy and energy decomposition analysis. In order to explore the interaction strength of the CL-20/HMX molecule and solvents, the cluster of cocrystal molecule and solvent molecules are built. First of all, we calculate the binding

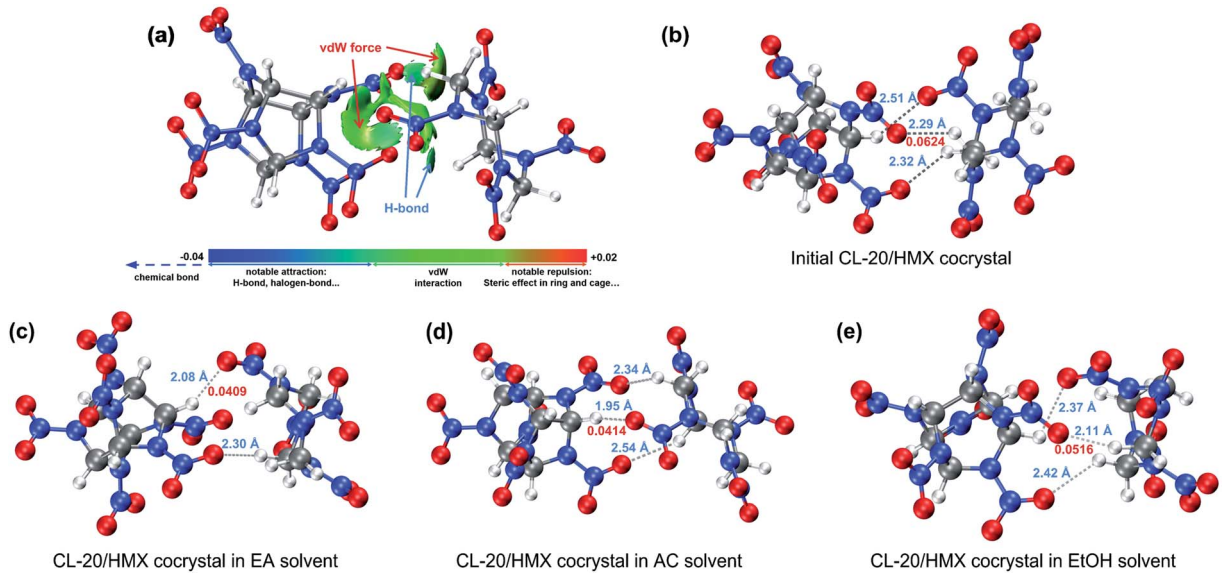

Fig. 2 (a) IRI maps with a color scale bar of CL-20/HMX cocrystal; (b–e) hydrogen bond structure of initial CL-20/HMX cocrystal and cocrystal in EA, AC and EtOH solvent. C, H, O, and N atoms are labeled as gray, white, red, and blue, respectively.

energy E_{bind} considering counterpoise correction of CL-20/HMX cocrystal and solvent. The binding energy considering counterpoise correction can be calculated by the total energies of the whole system and individual component energy in the system as follows:

$$E_{bind} = E_{cluster} - E_{cocrystal} - E_{solvent}$$

where $E_{cocrystal}$, $E_{solvent}$ and $E_{cluster}$ are energies of CL-20/HMX cocrystal molecule, solvent molecules and the cluster respectively, which are tabulated in Table 1. The E_{bind} of EA, AC and EtOH solvent are calculated to be -567.74 kJ mol^{-1}, -628.92 kJ mol^{-1} and -732.52 kJ mol^{-1} respectively. The larger binding energy means stronger intermolecular binding. During crystallization process, strong bound between crystal molecule and solvent will hinder the binding of free molecules to crystal surface.[43,54] Thus, the larger binding energy of solvent means the stronger hinder effect to the growth of cocrystal.

Combined with the energy decomposition based on molecular force field, the essence of the weak interaction between molecules can be investigated. As an important part of quantum chemistry analysis, energy composition can obtain the components of binding energy to analysis the interactions between fragments. The noncovalent interaction in the force field includes electrostatic and van der Waals interactions, in which van der Waals interaction can be divided into repulsion term and dispersion term. The bars with different colors in Fig. 3 represent different contributions of binding energy between CL-20/HMX cocrystal molecule and solvent molecules. The negative value means attraction and the positive value means repulsion. It can be seen that although the repulsion of AC is the largest among the three solvents, the absolute value of binding energy is lager than that of EA, meaning that electrostatic interaction and dispersion are still dominant. However, in EtOH solvent, the dispersion and repulsion are both the smallest, resulting in the strongest binding.

According to analysis of weak interaction, the hydrogen bond between CL-20 and HMX molecule is stronger in EA solvent. Meanwhile, it is evident from binding energy analysis of CL-20/HMX cocrystal molecules and solvent molecules that the binding between cocrystal and EA solvent is weak so that the

Table 1 Binding energy between CL-20/HMX cocrystal molecule and solvent molecules (kJ mol^{-1})

	$E_{cocrystal}$	$E_{solvent}$	$E_{cluster}$	E_{bind}
EA	−40110181.46	−7835351.28	−32274262.44	−567.74
AC	−28094699.19	−7835318.05	−20258752.21	−628.92
EtOH	−24096720.23	−7835328.92	−16260658.79	−732.52

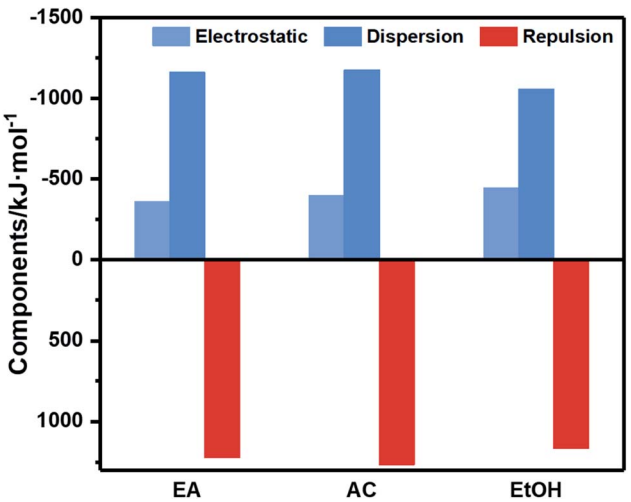

Fig. 3 Components of binding energy.

growth of cocrystal is less hindered by solvent. Thus, we can speculate that CL-20 molecules and HMX molecules are more likely to combine together to form cocrystal in EA solvent.

3.1.3 Analysis on CL-20/HMX/solvent mixture. XRD is an effective method to obtain the structure and composition information of crystal materials. Thus, in order to better simulate the combination of ε-CL-20 and β-HMX in solvent, we conduct the comparative analysis with XRD of CL-20/HMX cocrystal, as shown in Fig. 4(a) and (b). The crystal structures of ε-CL-20, β-HMX and CL-20/HMX cocrystal are shown in Fig. 4(c)–(e).

Due to the little change during crystallization, it is difficult to obtain detailed crystallization data by direct analysis of XRD pattern. Therefore, we quantitatively analyzed the XRD data, and calculated the percentage in forming CL-20/HMX cocrystal, ε-CL-20 and β-HMX, namely crystallization rate, as shown in Fig. 5.[32] It should be noted that, only the crystallization rate of the same crystal in different solvents can be compared, but the content of different crystals in the same solvent cannot be compared. It can be seen that the amount of cocrystal formed in EA solvent is the largest and that of EtOH is the least. However, in EtOH solvent, the solute molecules are more likely to form ε-CL-20 and β-HMX rather than cocrystal. According to the conjecture by analyzing the binding energy, the largest binding energy between CL-20/HMX cocrystal and EtOH molecules will inhibit the growth of cocrystal, representing a minor amount of cocrystal in solvent. The XRD results match with binding energy and confirm this conjecture.

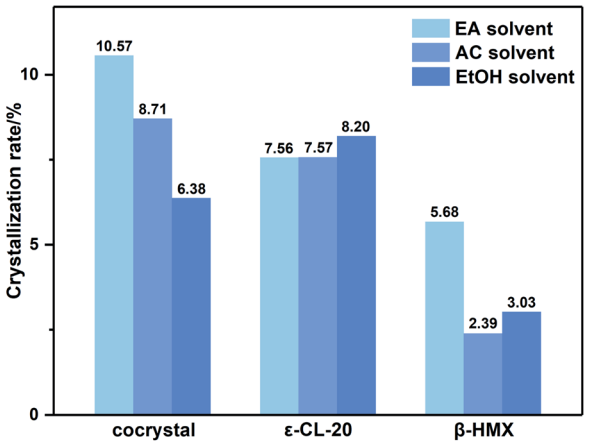

Fig. 5 Crystallization rate of CL-20/HMX/solvent mixtures.

3.1.4 Attachment energy. Attachment energy (AE) model is widely employed in the field of energetic materials due to its simple calculation steps and relatively reliable accuracy.[43,55,56] In vacuum, the attachment energy (E_{att}) is defined as the energy released when a growth slice added to a growing crystal surface, which can be calculated as follows:

$$E_{att} = E_{latt} - E_{slice}$$

where E_{latt} is the lattice energy of the cocrystal, and E_{slice} is the energy of a growth slice with thickness d_{hkl}. According to AE model, the growth rate (R_{hkl}) of crystal face is in directly proportion to the absolute value of attachment energy.

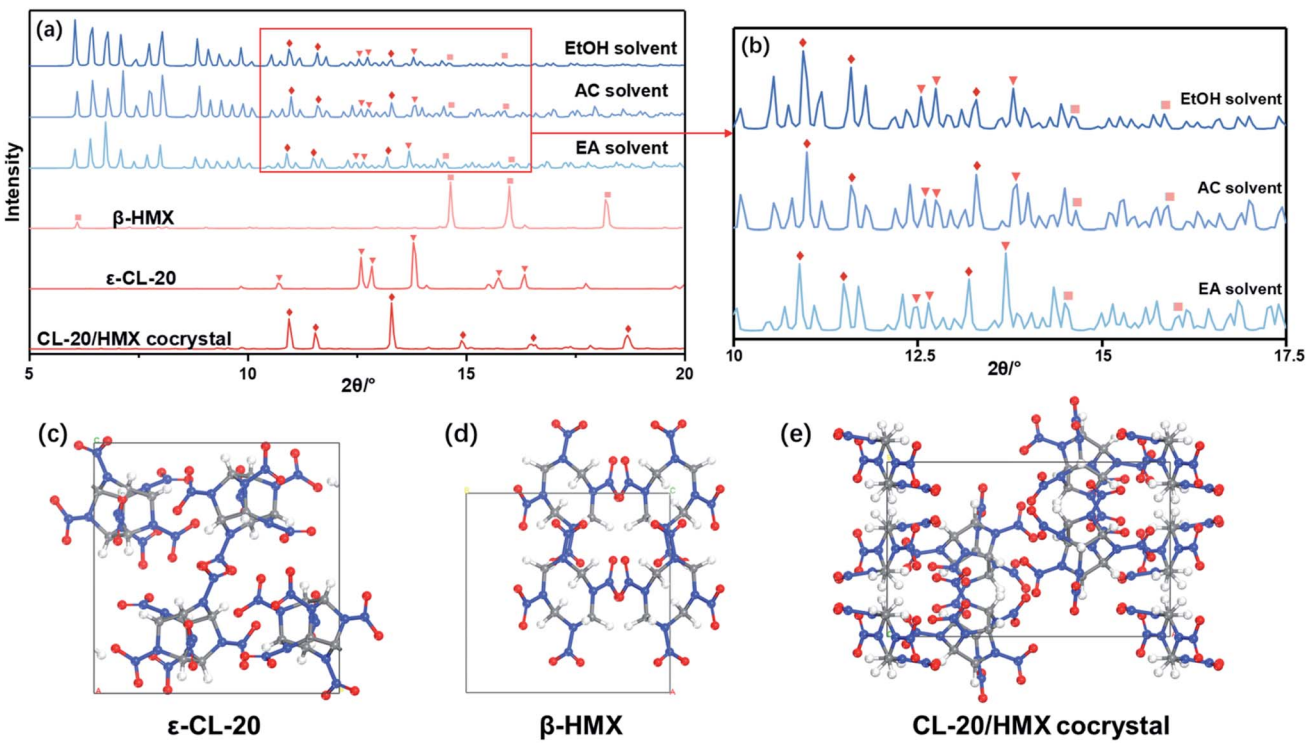

Fig. 4 (a) XRD patterns of CL-20/HMX/solvent mixtures; (b) insert of characteristic part of samples; (c–e) crystal structures of ε-CL-20, β-HMX and CL-20/HMX cocrystal. C, H, O, and N atoms are labeled as gray, white, red, and blue, respectively.

Table 2 Attachment energy and interaction energy of the cocrystal in vacuum and solvents (kJ mol^{-1})

	Vacuum	EA		AC		EtOH	
	E_{att}	E_{int}	E'_{att}	E_{int}	E'_{att}	E_{int}	E'_{att}
(1 0 0)	−1615.81	−398.88	248.39	−432.12	515.66	−444.86	634.09
(1 0 $\bar{2}$)	−5565.23	−898.97	−1362.08	−911.70	−1091.25	−981.07	−661.16
(1 1 0)	−4105.54	−656.80	−850.15	−712.21	−396.26	−838.31	345.02
(0 1 1)	−4575.21	−744.57	−681.64	−783.43	−268.85	−941.54	690.29
(1 1 1)	−4496.35	−809.20	−629.21	−842.71	−329.31	−938.64	209.37
(0 0 2)	−5773.66	−505.70	−3312.14	−511.28	−3194.47	−596.17	−2724.06

Meanwhile, the faster the growth rate, the easier it is to disappear in the growth process.

However, in solution, the growth rate is inhibited because of the adsorption of solvent molecules on crystal face. The attachment energy needs to be modified considering the solvent effect:

$$E'_{att} = E_{att} - E_s$$

where E_s means the effect of solvent adsorption on the energy term and can be calculated *via* the interaction energy (E_{int}) between solvent layer and the crystal face:

$$E_s = \frac{A_{acc}}{A_{box}} E_{int}$$

where A_{acc} is the solvent accessible area of the crystal face and A_{box} is the cross-section areas of crystal face in the simulation box. E_{int} can be defined as the difference between total energy of the crystal-solvent interface and the isolated component of crystal face (E_{cry}) and solvent layer (E_{sol}):

$$E_{int} = E_{total} - (E_{cry} + E_{sol})$$

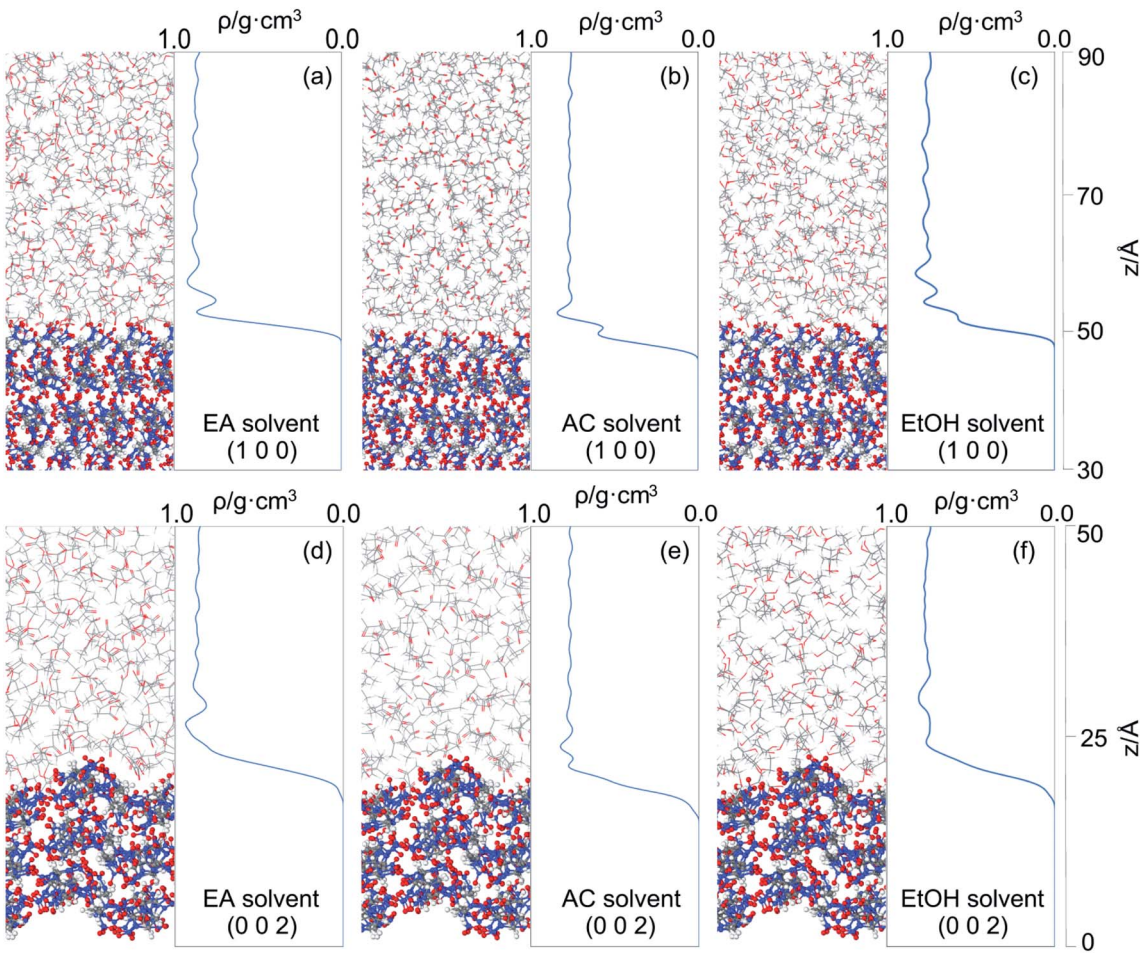

Fig. 6 Snapshots for the solvent-cocrystal interfacial structure and mass density distribution of solvent molecules: (a–c) EA, AC and EtOH solvent in (1 0 0) face; (d–f) EA, AC and EtOH solvent in (0 0 2) face. C, H, O, and N atoms are labeled as gray, white, red, and blue, respectively.

The E_{att} of the cocrystal in vacuum and solvents are shown in Table 2. It can be seen that, on the whole, the absolute value of attachment energy of EA is the largest and that of EtOH is the smallest, which meet the trend of the above analyses. Attachment energy is generally negative, a positive value indicates that the crystal face is unstable. Therefore, we can infer that CL-20 and HMX are less likely to form cocrystal in EtOH solvent.

3.1.5 Solvent distribution on cocrystal surface. The cocrystal-solvent interfacial structure was explored by mass density distribution perpendicular to the crystal face. Since the curves of five faces are similar, we mainly analyze the mass density distribution of (1 0 0) and (0 0 2) face, which have the largest and smallest E_{att}, in this paper. Layered arrangements of solvent molecules are observed in these two faces shown in Fig. 6.

It can be seen that more solvent molecules are concentrated at the peak nearest to the crystal surface, resulting in a higher local density than bulk density. The peaks of (1 0 0) are higher than that of (0 0 2), which means that the adsorption between solvent and crystal surface are stronger in (1 0 0) face. As we discussed above, the stronger bound of crystal and solvent, the slower growth of crystal face. This conclusion is consistent with the analysis of attachment energy. For different solvents, the behaviors of local density are not the same. Because of the smaller volume, AC and EtOH molecules are likely to adsorb in the pores on the crystal surface, leading to small peaks at 53 Å in (1 0 0) face, which also explains their higher interaction energy. When solvent molecules are away from the crystal face, the local mass density curve becomes flat in each system until it is close to the bulk density, indicating that the interactions of cocrystal face are negligible.

3.2 Experimental

3.2.1 XRD analysis. According to the theoretical calculation results, CL-20 and HMX are more inclined to form cocrystal in EA solvent. To test this, we did confirmatory experiments and characterized the samples obtained in different solvents by XRD. It can be seen in Fig. 7 that CL-20/HMX cocrystals are generated clearly both in EA and AC solvent, but there is almost no characteristic peak of cocrystal in EtOH solvent.

Table 3 The relative content of each phase in different solvents (%)

Samples	EA	AC	EtOH
Cocrystal	75.05	62.52	3.34
ε-CL-20	15.88	24.46	58.63
β-HMX	8.60	11.80	13.87

In order to explore the crystallization behavior of ε-CL-20 and β-HMX in different solvents more accurately, the XRD quantitative analysis method is employed in this experiment. The relative contents of each phase in the samples are shown in Table 3. It can be seen that, the relative content of CL-20/HMX cocrystal in EA solvent reaches 75.05%, which is the most in these samples. The rank of cocrystal content is EA > AC > EtOH, which is consistent well with the theoretical calculation result in Section 3.1.3. However, the ranks of contents of ε-CL-20 and β-HMX are not very agree with the calculation result. It may be because the crystal phases are more complex and the molecules may exist in the CL-20/HMX/solvent mixture in an amorphous form but we can obtain only one of the crystal phases.

From macro perspective, the cocrystallization rate is higher in EA solvent, which is well confirmed by theoretical calculations and experiments. The polarity order of these three solvents is EA < AC < EtOH. Therefore, we speculate that the different performance of cocrystal is related to polarity of solvents.

3.2.2 Morphology analysis. According to the modified AE model, the growth rate of crystal face in solution is still proportional to E'_{att}. Therefore, the crystal morphology grown in solution can be obtained *via* the growth rate of each crystal face, as shown in Fig. 8(a)–(c). It can be seen that the influence of solvent on the crystal face will lead to the difference of attachment energy, which macro performs in the difference of crystal morphology. Because some cocrystal faces have pores that can hold small molecules, small-volume solvent like AC and EtOH

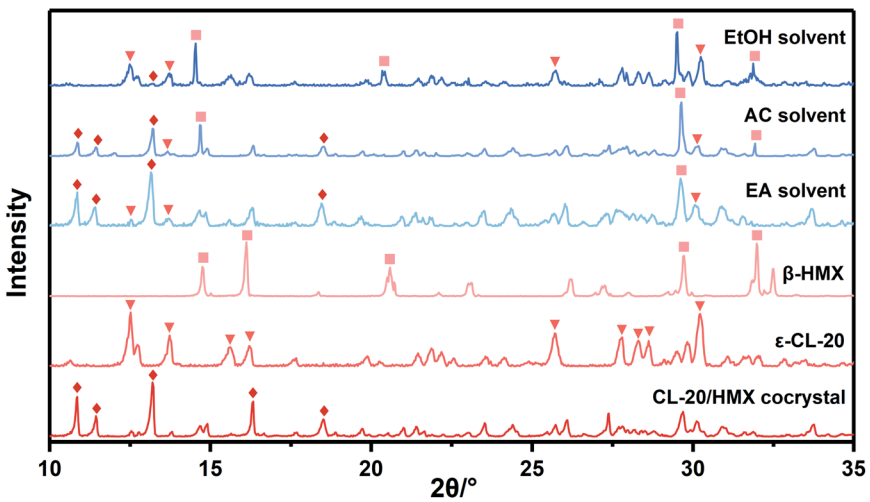

Fig. 7 XRD patterns of CL-20/HMX cocrystal in different solvents.

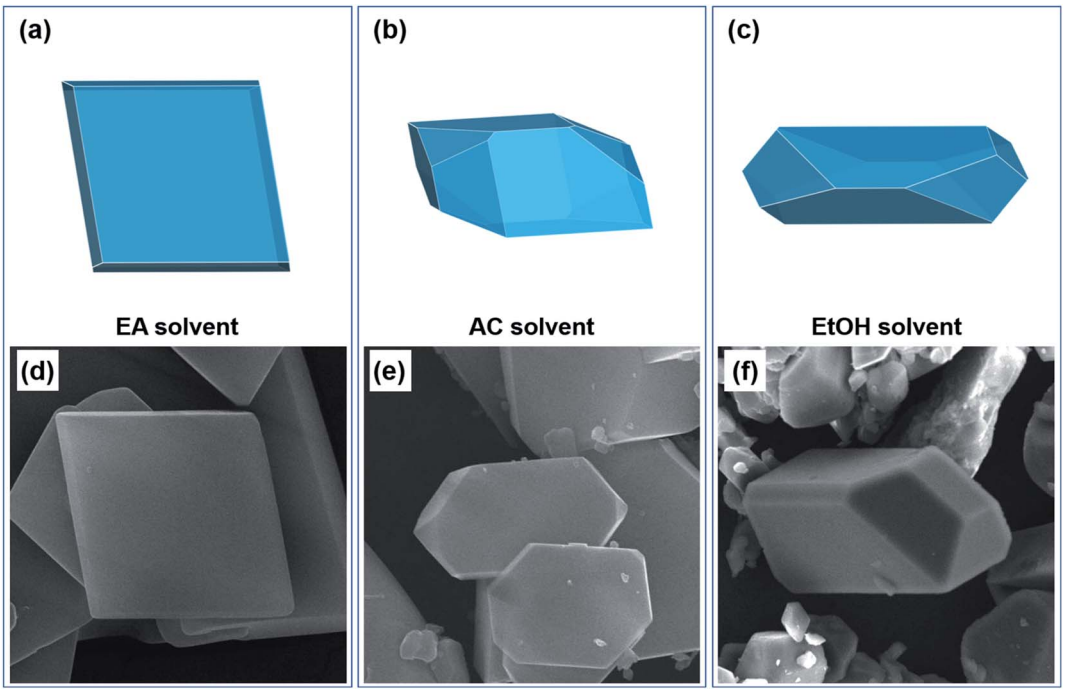

Fig. 8 (a–c) The predicted morphology and (d–f) SEM image of CL-20/HMX cocrystal in EA, AC and EtOH solvent.

can adsorb tight on these faces. Thus, the interaction energies of these solvent-cocrystal interface are relatively high, leading to a small attachment energy and slow growth rate. The faster the growth of the crystal face, the easier it will disappear in crystallization process, leading to a wide range of morphology.

At the same time, the samples prepared in the experiments were characterized by SEM, as shown in Fig. 8(d)–(f). It is evident from the figures that the predicted shapes of CL-20/HMX cocrystal in EA and EtOH solvent are in good agreement with the experimental results of cocrystallization. In EA solvent, CL-20 and HMX tend to grow into quadrilateral sheet cocrystal but grow much slenderer into rodlike cocrystal in EtOH solvent. However, in AC solvent, there is a big gap between the predicted morphology and the experiment. It might because the volatilization rate of AC solvent is too fast, the complex dynamic influence leads to the deflection of the prediction results.

4 Conclusions

In this work, we mainly studied the cocrystallization performance and mechanism of CL-20 and HMX in EA, AC and EtOH solvents through theoretical calculations and experiments. In conclusion, analysis of the weak interaction and binding energy showed that in EA solvent, CL-20 and HMX tend to be combined together and there is less hindered by solvent molecules. Analysis on CL-20/HMX/solvent mixture and mass density distribution showed that the cocrystallization rate of CL-20 and HMX is the highest in EA solvent and the solvent effect has a great influence on crystal faces. More importantly, these theoretical results are well confirmed by XRD and SEM experiments. On the basis of this, we find low-polarity solvent are easy to form cocrystal, which morphology is controllable. We believe that combined with various calculation methods and experimental verification, the solvent suitable for cocrystal preparation can be effectively selected and it will make access to excellent cocrystal more efficient.

Conflicts of interest

There are no conflicts to declare.

Acknowledgements

This work was financially supported by the National Natural Science Foundation of China (21975150).

References

1 R. L. Simpson, P. A. Urtiew, D. L. Ornellas, G. L. Moody, K. J. Scribner and D. M. Hoffman, *Propellants, Explos., Pyrotech.*, 1997, **22**, 249–255.
2 U. R. Nair, R. Sivabalan, G. M. Gore, M. Geetha, S. N. Asthana and H. Singh, *Combust., Explos. Shock Waves*, 2005, **41**, 121–132.
3 G. Li, J. Wang, X. Ren and J. He, *J. Solid Rocket Technol.*, 2021, **44**, 622–629.
4 Y. Ma, A. Zhang, X. Xue, D. Jiang, Y. Zhu and C. Zhang, *Cryst. Growth Des.*, 2014, **14**, 6101–6114.
5 I. D. H. Oswald, W. D. S. Motherwell and S. Parsons, *Acta Crystallogr., Sect. E: Struct. Rep. Online*, 2004, **60**, o1967–o1969.
6 O. Bolton, L. R. Simke, P. F. Pagoria and A. J. Matzger, *Cryst. Growth Des.*, 2012, **12**, 4311–4314.

7 K. B. Landenberger and A. J. Matzger, *Cryst. Growth Des.*, 2010, **10**, 5341–5347.
8 O. Bolton and A. J. Matzger, *Angew. Chem., Int. Ed.*, 2011, **50**, 8960–8963.
9 H. Gao, W. Jiang, J. Liu, G. Hao, L. Xiao, X. Ke and T. Chen, *J. Energy Mater.*, 2017, **35**, 490–498.
10 H. Xu, X. Duan, H. Li and C. Pei, *RSC Adv.*, 2015, **5**, 95764–95770.
11 H. Lin, S.-G. Zhu, L. Zhang, X.-H. Peng, P.-Y. Chen and H.-Z. Li, *Int. J. Quantum Chem.*, 2013, **113**, 1591–1599.
12 S. Zhu, S. Zhang, R. Gou, G. Han, C. Wu and F. Ren, *J. Mol. Model.*, 2017, **23**, 353.
13 X. Ding, R.-J. Gou, F.-D. Ren, F. Liu, S.-H. Zhang and H.-F. Gao, *Int. J. Quantum Chem.*, 2016, **116**, 88–96.
14 C. Guo, H. Zhang, X. Wang, J. Xu, Y. Liu, X. Liu, H. Huang and J. Sun, *J. Mol. Struct.*, 2013, **1048**, 267–273.
15 Y. Wang, Z. Yang, H. Li, J. Wang, X. Zhou and Q. Zhang, *Chin. J. Energ. Mater.*, 2013, **21**, 554–555.
16 S. Yuan, B. Gou, S. Guo, L. Xiao, Y. Hu, T. Chen, G. Hao and W. Jiang, *Chin. J. Explos. Propellants*, 2020, **43**, 167–172.
17 Y. Shu, Z. Wu, N. Liu, X. Ding, M. Wu, K. Wang and Y. Lu, *Chin. J. Explos. Propellants*, 2015, **38**, 1–9.
18 W. Wei, W. Chen, L. Mi, J. Xu and J. Zhang, *J. Mater. Chem. A*, 2021, **9**, 23860–23872.
19 T. Sun, J. J. Xiao, Q. Liu, F. Zhao and H. M. Xiao, *J. Mater. Chem. A*, 2014, **2**, 13898–13904.
20 D. Musumeci, C. A. Hunter, R. Prohens, S. Scuderi and J. F. McCabe, *Chem. Sci.*, 2011, **2**, 883.
21 H. Gao, S. Zhang, F. Ren, F. Liu, R. Gou and X. Ding, *Comput. Mater. Sci.*, 2015, **107**, 33–41.
22 H. Li, Y. Shu, S. Gao, L. Chen, Q. Ma and X. Ju, *J. Mol. Model.*, 2013, **19**, 4909–4917.
23 R. Feng, S. Zhang, F. Ren, R. Gou and L. Gao, *J. Mol. Model.*, 2016, **22**, 123.
24 X. Song, Y. Wang, S. Zhao and F. Li, *RSC Adv.*, 2018, **8**, 34126–34135.
25 G. Hang, W. Yu, T. Wang, J. Wang and Z. Li, *J. Mol. Struct.*, 2017, **1141**, 577–583.
26 W. Wei, J. Wu, S. Cui, Y. Zhao, W. Chen and L. Mi, *Nanoscale*, 2019, **11**, 6243–6253.
27 Z. Wu, Y. Shu, N. Liu, X. Ding, M. Wu, K. Wang and Y. Lu, *Chin. J. Explos. Propellants*, 2016, **39**, 37–42.
28 X. Zhao, X. Fu, L. Lin, J. Li, L. Jiang and X. Fan, *J. Ordnance Equip. Eng.*, 2022, **43**, 11–21.
29 G. F. Ji, H. M. Xiao and H. S. Dong, *Acta Chim. Sin.*, 2002, **60**, 194–199.
30 T. D. Sewell, R. Menikoff, D. Bedrov and G. D. Smith, *J. Chem. Phys.*, 2003, **119**, 7417–7426.
31 S. Sun, H. Zhang, Y. Liu, J. Xu, S. Huang, S. Wang and J. Sun, *Cryst. Growth Des.*, 2018, **18**, 77–84.
32 X. Zhao, X. Fu, G. Zhang, X. Liu and X. Fan, *ACS Omega*, 2022, **7**, 7361–7369.
33 T. Lu, *Molclus program, Version 1.9.9.7*, **https://www.keinsci.com/research/molclus.html**, accessed December 2021.
34 S. Grimme, C. Bannwarth and P. Shushkov, *J. Chem. Theory Comput.*, 2017, **13**, 1989–2009.
35 C. Bannwarth, S. Ehlert and S. Grimme, *J. Chem. Theory Comput.*, 2019, **15**, 1652–1671.
36 S. Grimme, S. Ehrlich and L. Goerigk, *J. Comput. Chem.*, 2011, **32**, 1456–1465.
37 S. Grimme, J. Antony, S. Ehrlich and H. Krieg, *J. Chem. Phys.*, 2010, **132**, 154104.
38 P. J. Stephens, F. J. Devlin, C. F. Chabalowski and M. J. Frisch, *J. Phys. Chem.*, 1994, **98**, 11623–11627.
39 D. Rappoport and F. Furche, *J. Chem. Phys.*, 2010, **133**, 134105.
40 J. Zheng, X. Xu and D. G. Truhlar, *Theor. Chem. Acc.*, 2011, **128**, 295–305.
41 T. Lu, Z. Liu and Q. Chen, *Mater. Sci. Eng., B*, 2021, **273**, 115425.
42 W. Humphrey, A. Dalke and K. Schulten, *J. Mol. Graphics*, 1996, **14**(33–38), 27–28.
43 Y. Liu, *Chin. J. Explos. Propellants*, 2021, **44**, 578–588.
44 H. Sun, P. Ren and J. R. Fried, *Comput. Theor. Polym. Sci.*, 1998, **8**, 229–246.
45 H. Sun, *J. Phys. Chem. B*, 1998, **102**, 7338–7364.
46 S. W. Bunte and H. Sun, *J. Phys. Chem. B*, 2000, **104**, 2477–2489.
47 H. C. Andersen, *J. Chem. Phys.*, 1980, **72**, 2384–2393.
48 B. M. Moshtaghioun and A. Monshi, *J. Mater. Process. Technol.*, 2008, **196**, 52–63.
49 P. J. Williams, J. J. Biernacki, J. Bai and C. J. Rawn, *Cem. Concr. Res.*, 2003, **33**, 1553–1559.
50 T. Lu and Q. Chen, *Chemistry–Methods*, 2021, **1**, 231–239.
51 S. Emamian, T. Lu, H. Kruse and H. Emamian, *J. Comput. Chem.*, 2019, **40**, 2868–2881.
52 F. Fuster and B. Silvi, *Theor. Chem. Acc.*, 2000, **104**, 13–21.
53 S. J. Grabowski, *Chem. Rev.*, 2011, **111**, 2597–2625.
54 Y. Liu, T. Yu, W. Lai, Y. Ma, Y. Cao, N. Liu, Z. Ge and F. Zhao, *Cryst. Growth Des.*, 2020, **20**, 521–524.
55 Z. Berkovitch-Yellin, *J. Am. Chem. Soc.*, 1985, **107**, 8239–8253.
56 R. Docherty, G. Clydesdale, K. J. Roberts and P. Bennema, *J. Phys. Appl. Phys.*, 1991, **24**, 89–99.